Characteristics of the 15-year surge of Mittie Glacier, SE Ellesmere Island, Canadian Arctic

Luke Copland[1] (ID), Danielle Hallé[2] (ID), Wesley Van Wychen[2] (ID), Benoît Lauzon[1] (ID), Julian A. Dowdeswell[3] and Jamie Davis[4]

[1]Department of Geography, Environment and Geomatics, University of Ottawa, Ottawa, ON K1N 6N5, Canada; [2]Department of Geography and Environmental Management, University of Waterloo, Waterloo, ON N2L 3G1, Canada; [3]Scott Polar Research Institute, University of Cambridge, Cambridge CB2 1ER, UK and [4]Department of Earth and Atmospheric Sciences, University of Alberta, Edmonton, AB T6G 2E3, Canada

Abstract

A surge of Mittie Glacier, a 50 km-long tidewater outlet glacier of Manson Icefield, occurred between approximately 1992 and 2007. Velocities increased slowly at first, but then increased rapidly to reach a peak of 4800 m a^{-1} in early 1996, the highest ever reported for a glacier in the Canadian Arctic. The surge initiated at the terminus and propagated up-glacier, with a maximum terminus advance of 7.3 km between 1994 and 1999. The surge was almost entirely restricted to the lower ∼30 km of the glacier, in a region which radio-echo sounding shows to be grounded below sea level. A 3 km-wide crevasse with a 150 m opening occurred at the separation between faster moving ice downstream and slower moving ice upstream. Surge initiation appears to have been triggered by flotation of the lower terminus, caused by long-term thinning of this region during quiescence.

1. Introduction

Glaciers in the Canadian Arctic demonstrate significant variations in velocity on timescales ranging from days (Iken, 1974; Copland and others, 2003*b*), to seasons (Bingham and others, 2003; Thomson and Copland, 2018), to multi-annual to decadal periods (Heid and Kääb, 2012; Van Wychen and others, 2016, 2021; Schaffer and others, 2017; Thomson and Copland, 2018). Sub-annual variations appear to be driven primarily by changes in the volume and timing of water flow to the glacier bed and can cause velocities to increase by 100% or more above winter values for short periods (Iken, 1974; Thomson and Copland, 2018). Longer-term variations have taken several forms: gradual long-term slowdowns primarily driven by changes in ice thickness (Schaffer and others, 2017; Thomson and Copland, 2018), long-term speed-ups driven by changes in subglacial conditions (Harcourt and others, 2020; Dalton and others, 2022) or mass balance/surging (Medrzycka and others, 2019; Lauzon and others, 2024), and rapid speed-ups and slowdowns driven by glacier surging or pulsing (Copland and others, 2003*a*; Van Wychen and others, 2016, 2021, 2022; Lauzon and others, 2023). Given strongly negative surface mass balances over Canadian Arctic ice caps over the past few decades (Noël and others, 2018; Ciracì and others, 2020; Hugonnet and others, 2021), and predictions of continued losses into the future (Lenaerts and others, 2013), a major unresolved question is how glacier velocities will respond in a warming climate, including whether the frequency, duration and magnitude of glacier surging will change (Dowdeswell and others, 1995). We also do not have a good understanding of the factors that cause glaciers to surge in the Canadian Arctic, and the timescales over which these factors operate.

Surge-type glaciers experience non-uniform velocity variations that consist of active and quiescent phases (Meier and Post, 1969). The active phase is a period when a glacier's velocity typically increases by an order of magnitude or more above background levels and can last from years to a decade or longer on polythermal glaciers in the Arctic (Dowdeswell and others, 1991; Murray and others, 2003). This is followed by a quiescent phase during which glacier velocity returns to a slow or stagnant levels, which can last from decades to a century or longer. Surge-type glaciers can be identified through characteristics such as rapid terminus advance, high surface velocities, widespread crevassing, rapid changes in surface elevation and looped moraines during the active phase (Meier and Post, 1969; Copland and others, 2003*a*). The quiescent phase often shows stagnant ice and potholes on the glacier surface, together with low velocities.

The first reports of glacier surging in the Canadian Queen Elizabeth Islands (QEI) are from the 1960s (Hattersley-Smith, 1964, 1969; Müller, 1969; Ommanney, 1969), and include descriptions of terminus advance of up to 6 km, intense surface crevassing and velocities of up to 7.7 m d^{-1} (∼2800 m a^{-1}) for Otto Glacier on northern Ellesmere Island (Hattersley-Smith, 1969). The first systematic review of surge-type glaciers in the QEI was undertaken by Copland and others (2003*a*), who identified a total of 51 surge-type glaciers based on the criteria described above, with 15 glaciers actively surging in 1999/2000. This is one of the highest concentrations of surge-type glaciers for any region in the Arctic, with perhaps only more being found in Svalbard (Sevestre and Benn, 2015). The largest active surge reported by Copland and others (2003*a*) was of Mittie Glacier, southeast Ellesmere Island, which was observed to

be flowing at >1 km a^{-1}, and had advanced by ∼4 km into marine waters since its last recorded position in 1959.

A major impediment to understanding surging glacier dynamics in the QEI is that little previous analysis has been undertaken of the full active phase of a surge in this region. The only such study is that of Lauzon and others (2023), who described the 22-year long surge of Iceberg Glacier, western Axel Heiberg Island, >400 km NW of our study location. Here we describe the complete surge cycle of Mittie Glacier using changes in terminus position and surface characteristics since 1972, changes in surface velocity on a near-annual basis since the late 1980s and temporal trends in backscatter values in synthetic aperture radar (SAR) imagery. Our findings provide information about the duration of the active phase, the evolution of surface velocities during a surge, the location of surge initiation and termination, and insights into the controls on glacier surging in the Canadian Arctic.

2. Study area

Mittie Glacier (76.87°N, 79.09°W) is the largest marine-terminating outlet of Manson Icefield on Ellesmere Island and is ∼50 km long and up to ∼9 km wide at its terminus (Fig. 1). It terminates in Smith Bay, which is connected to northern Baffin Bay. Mittie Glacier flows generally northward, contains four main tributary glaciers and has a total drainage area of ∼2000 km^2 (Copland and others, 2003*a*). Previous studies have described Mittie Glacier during the active phase of the surge cycle, with peak velocities of >1300 m a^{-1} recorded in 1999–2000 (Copland and others, 2003*a*), and >700 m a^{-1} in 2004–2005 (Sharp and others, 2014), with a general increase in velocity towards the terminus. The north and east sides of Manson Icefield contain the highest concentration of surge-type glaciers in the Canadian Arctic (Sharp and others, 2014), with Copland and others (2003*a*) identifying six glaciers there as surge-type, including Mittie Glacier.

Van Wychen and others (2016) computed a mass flux of 0.90 ± 0.25 Gt a^{-1} for the terminus of Mittie Glacier in 2000, compared to 0.09 ± 0.05 Gt a^{-1} for 2007 and 0.02 ± 0.02 Gt a^{-1} for 2012–2015. Similarly, Millan and others (2017) quantified the mass flux of Mittie Glacier to be 0.9 ± 0.01 Gt a^{-1} for 2000, compared to a mean of 0.02 ± 0.002 Gt a^{-1} over the period 2003–2015. The flux in 2000 comprised over 25% of total QEI ice discharge to the ocean of 3.5 ± 0.5 Gt a^{-1} for that year (Millan and others, 2017).

3. Methods and data

3.1. Terminus position and surface characteristics

A combination of SAR and optical images was used to map the location of the terminus and surface features of Mittie Glacier at approximately 5-year intervals between 1972 and 1992, and on an annual basis between 1992 and 2017 (Table 1). Optical imagery was acquired by Landsat 1–5 MSS/TM, Landsat 7 ETM + and Landsat 8 OLI sensors, and downloaded from the United States Geological Survey EarthExplorer (https://earthexplorer.usgs.gov/). SAR imagery was acquired by ERS-1, ERS-2, JERS-1 and ALOS PALSAR, and downloaded from the Alaska Satellite Facility (https://search.asf.alaska.edu/).

Both SAR and optical images were used to manually outline the terminus of Mittie Glacier, to track its change in position over time, and to determine changes in surface features and velocities. The east and west sides of the terminus did not change in the same way, so were assessed separately in relation to their respective maximum extent (delineation between east and west
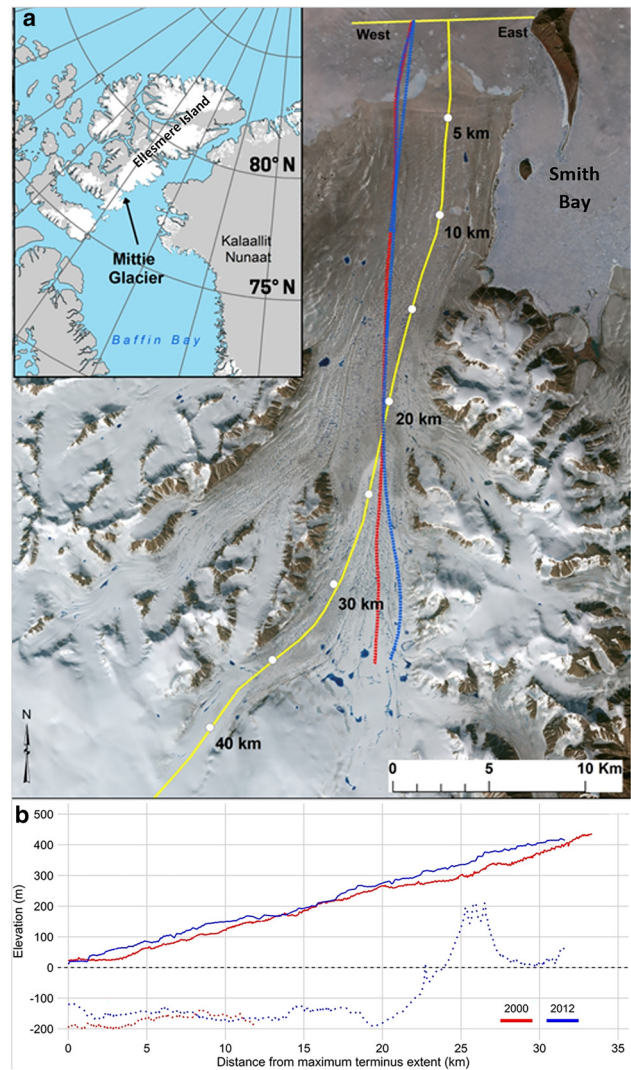

Figure 1. (a) Overview of Mittie Glacier, with yellow line indicating centreline profile used for surface velocity measurements, and red and blue lines indicating location of 2000 and 2012 airborne radar ice thickness measurements, respectively. Background: SPOT5, 17 July 2009. Inset map: location of Mittie Glacier on southeast Ellesmere Island. (b) Surface and glacier bottom elevations from airborne radar measurements, following the flightlines shown in (a).

indicated by yellow line in Fig. 1). Optical imagery was used to identify surface characteristics that are distinctive for surge-type glaciers, such as extensive crevassing and rapid terminus advance during the active phase, and potholes and surface ponding during the quiescent phase (Copland and others, 2003*a*). Backscatter in SAR imagery was used to determine surge onset and extent, as increases in crevassing caused by rapid changes in ice motion are detectable as changes in surface roughness (Colgan and others, 2016; Kääb and others, 2023). This is most effectively seen in winter when the glacier surface is cold and dry, but returns from crevasses can still be seen in the summer when the surface is wet and backscatter is typically lower. The SAR images also helped to identify other features indicative of surging, such as highly crevassed shear margins with bright backscatter in locations of high-velocity contrast.

3.2. Surface velocities

The earliest surface velocities of Mittie Glacier were provided by the NASA MEaSUREs Inter-mission Time Series of Land Ice Velocity and Elevation (ITS_LIVE) project (Gardner and others,

Table 1. Details of imagery used in this study to determine terminus position and surface characteristics of Mittie Glacier

Sensor	Scene ID	Date (dd/mm/yyyy)	Resolution (m)
ERS-1	E1_04614_STD_F195	03/06/1992	12.5
ERS-1	E1_06661_STD_F195	24/10/1992	12.5
ERS-1	E1_11399_STD_F195	20/09/1993	12.5
ERS-1	E1_12673_STD_F195	18/12/1993	12.5
ERS-1	E1_15297_STD_F195	19/06/1994	12.5
JERS-1	J1_16814_STD_F25	09/03/1995	12.5
ERS-1	E1_24225_STD_F195	03/03/1996	12.5
ERS-2	E2_04552_STD_F195	04/03/1996	12.5
ERS-1	E1_24268_STD_F195	06/03/1996	12.5
ERS-2	E2_04595_STD_F195	07/03/1996	12.5
ERS-1	E1_25499_STD_F195	31/05/1996	12.5
ERS-2	E2_17578_STD_F195	31/08/1998	12.5
ERS-2	E2_27598_STD_F195	31/07/2000	12.5
ERS-2	E2_43358_STD_F196	06/08/2003	12.5
ALOS PALSAR	ALPSRP046101540	06/12/2006	12.5
Landsat 1 MSS	LM10420051972257PAC01	13/09/1972	60
Landsat 1 MSS	LM10460041975173PAC01	22/09/1975	60
Landsat 2 MSS	LM20440051980244PAC01	01/09/1980	60
Landsat 5 MSS	LM50400051985193PAC01	12/07/1985	60
Landsat 5 MSS	LM50400051992261PAC01	18/09/1992	30
Landsat 5 TM	LT50410051993190PAC00	09/07/1993	30
Landsat 5 MSS	LM50360061994254PAC01	11/09/1994	30
Landsat 5 TM	LT05_L1GS_036006_19970327_20170101_01_T2	27/03/1997	30
Landsat 5 TM	LT50360061998249PAC00	06/09/1998	30
Landsat 5 TM	LT50360061999204PAC00	23/07/1999	30
Landsat 7 ETM+	LE07_L1TP_036006_20000903_20170210_01_T1	28/08/2000	15
Landsat 7 ETM+	LE70360062001201EDC00	20/07/2001	15
Landsat 7 ETM+	LE70400052002200EDC00	08/08/2002	15
Landsat 5 TM	LT50360062003263PAC00	20/09/2003	15
Landsat 7 ETM+	LE70380052004192EDC02	11/07/2004	15
Landsat 7 ETM+	LE70360062005212EDC00	31/07/2005	15
Landsat 7 ETM+	LE70380052007232EDC00	20/08/2007	15
Landsat 7 ETM+	LE07_L1TP_038005_20080705_20161228_01_T1	05/07/2008	15
Landsat 7 ETM+	LE70390052009212EDC00	31/07/2009	15
Landsat 7 ETM+	LE70390052010183EDC01	02/07/2010	15
Landsat 7 ETM+	LE70390052011186EDC01	05/07/2011	15
Landsat 7 ETM+	LE70360062012200ASN00	20/07/2012	15
Landsat 7 ETM+	LE70390052013191ASN00	10/07/2013	15
Landsat 7 ETM+	LE70380052014187EDC00	06/07/2014	15
Landsat 8 OLI	LC80410052015203LGN00	22/07/2015	15
Landsat 8 OLI	LC80360062016219LGN00	07/07/2016	15
Landsat 8 OLI	LC08_L1TP_038005_20170924_20171013_01_T1	24/09/2017	15

2021; https://its-live.jpl.nasa.gov/), for 1988, 1989, 1990, 1991 and 1992, as well as for 2010 and 2018. We used the regional velocity mosaic product, which provides near-complete coverage of the glacier at 240 m resolution, derived from processing of all Landsat image pairs with the auto-RIFT feature tracking algorithm (Gardner and others, 2018). Errors are provided for each pixel in the ITS_LIVE velocity mosaics, and typically average ~5–20 m a^{-1} across Mittie Glacier.

From 1996 onwards most surface velocities were derived from our own processing, due to lack of coverage in the ITS_LIVE dataset during the main surge (likely due to low coherence between images caused by extensive surface crevassing), and to enable mapping at higher resolutions. Velocities in 1996 were derived from offset tracking of a pair of ERS 1/2 images collected on 3 and 4 March 1996, using GAMMA software (Strozzi and others, 2002, Werner and others, 2005) (Table 2). Geocoding of these scenes was undertaken using the ArcticDEM (https://www.pgc. umn.edu/data/arcticdem/), with velocities derived at a resolution of 20 m. Errors are estimated to be 2 m d^{-1}.

Annual velocities from 1999 to 2010 were derived from feature tracking of pairs of summer Landsat 7 ETM+ images with a MATLAB cross-correlation algorithm implemented in the frequency domain. The images were first coregistered to a common base image from 2000, and then a variable correlation block size was used to find the optimum match between image pairs. This method provides a good way to determine ice motion in regions with strong spatial gradients (e.g. near glacier margins), and is fully described in Van Wychen and others (2016). Following the methodology of Van Wychen and others (2016), errors in the feature tracking were assessed from apparent motion over stationary bedrock locations (maximum 0.75 pixel = 11.25 m), and the ability of the algorithm to pick the subpixel location of the correlation peak (~0.5 pixel = 7.5 m). These errors are considered to be independent, so the total average error for the feature tracking velocities is estimated to be ± 19 m a^{-1}.

Velocities from winter 2012, 2013, 2015, 2016 and 2018 were derived from speckle tracking of pairs of co-registered Radarsat 2 fine beam (9 m resolution) images collected on repeat orbits with 24-day separation (Table 2). These were processed with a custom-written code in MATLAB (Short and Gray, 2005; Van Wychen and others, 2014, 2016), which uses a cross-correlation algorithm on overlapping image chips of 101 pixels in azimuth and range direction. The Canadian Digital Elevation Dataset (scale 1: 250 000) was used to remove the range shift component from these results, and displacements were calibrated over bedrock outcrops with zero motion to remove any systematic bias. Errors in the speckle tracking results were determined from apparent motion over stationary bedrock locations and ice divides, which ranged between an average of 3.7 and 21.1 m a^{-1} for Manson Icefield, depending on year (Van Wychen and others, 2016). The root sum of squares from all Radarsat 2 velocity derivations was ±8.7 m a^{-1}, which we consider to be our average speckle tracking velocity error.

Table 2. Details of imagery used in this study to derive surface velocities of Mittie Glacier

Period	Image 1 (dd/mm/yyyy), image ID or path-row	Image 2 (dd/mm/yyyy), image ID or path-row	Sensor(s)
1988 annual	ITS_LIVE composite	N/A	Landsat 4 and 5
1989 annual	ITS_LIVE composite	N/A	Landsat 4 and 5
1991 annual	ITS_LIVE composite	N/A	Landsat 4 and 5
1992 annual	ITS_LIVE composite	N/A	Landsat 4 and 5
1996 winter	03/03/1996, E1_24225_STD_F195	03/04/1996, E2_04552_STD_F195	ERS-1, ERS-2
1999–2000	13/07/1999, 38–5	29/06/2000, 38–5	Landsat 7
2000–2001	11/06/2000, 40–5	14/06/2001, 40–5	Landsat 7
2001–2002	14/06/2001, 40–5	10/06/2002, 39–5	Landsat 7
2002–2003	19/07/2002, 40–5	11/08/2003, 36–6	Landsat 7
2003–2004	11/08/2003, 36–6	17/07/2004, 39–5	Landsat 7
2004–2005	17/07/2004, 39–5	04/07/2005, 38–5	Landsat 7
2005–2006	04/07/2005, 38–5	30/06/2006, 38–5	Landsat 7
2006–2007	30/06/2006, 38–5	03/07/2007, 38–5	Landsat 7
2007–2008	03/07/2007, 38–5	05/07/2008, 38–5	Landsat 7
2008–2009	21/07/2008, 38–5	22/07/2009, 40–5	Landsat 7
2009–2010	29/06/2009, 39–5	23/06/2010, 40–5	Landsat 7
2010 annual	ITS_LIVE composite	N/A	Landsat 5 and 7
2012 winter	09/04/2012	03/05/2012	Radarsat 2
2013 winter	05/01/2013	29/01/2013	Radarsat 2
2015 winter	12/02/2015	08/03/2015	Radarsat 2
2016 winter	14/01/2016	07/02/2016	Radarsat 2
2018 winter	03/01/2017	27/01/2017	Radarsat 2
2018 annual	ITS_LIVE composite	N/A	Landsat 7 and 8

For plotting, velocity outputs were imported into ArcMap 10.7.1, displacements were standardized to annual values, and bedrock locations masked out. The velocity maps were filtered manually to remove erroneous values, which were identified following the methodology of Van Wychen and others (2014, 2016, 2021):

(1) Velocity vectors should generally follow the direction of surface characteristics such as lateral and medial moraines;
(2) The magnitude and orientation of velocities should not change dramatically over a short distance;
(3) Velocities are typically greater in the centre of the glacier than at the margins.

In this study, we compare velocities determined over relatively short periods in the winter (from SAR offset tracking and speckle tracking), to velocities determined over multi-week to annual periods (from optical feature tracking), so it is important to understand whether there is seasonal variability in motion. In the study of Van Wychen and others (2014), a comparison of continuous dual-frequency Global Positioning System (dGPS) measurements at tidewater Belcher Glacier, Devon Ice Cap (~150 km south of Mittie Glacier), suggested that annual velocities were ~10–15% faster than winter velocities. For the QEI as a whole, Van Wychen and others (2016) compared >970 000 velocity points over tidewater glaciers derived from overlapping regions in speckle tracking and feature tracking imagery and determined that winter velocities were on average 13.6% lower than annual velocities. It is unknown whether similar seasonal variability occurs on surge-type glaciers, but to be conservative we only considered velocity changes to be significant if they were >15% different between datasets, regardless of the time of year of their acquisition.

3.3. Surface and bed topography

Ice thickness data for Mittie Glacier were collected during two airborne missions. The first was flown by the Scott Polar Research Institute (SPRI), University of Cambridge, in April 2000 using a 100 MHz radio-echo sounding system mounted on a Twin Otter aircraft flying at an average air speed of ~230 km h^{-1} (Fig. 1). Aircraft positioning was determined from dGPS measurements, with average horizontal errors of ~5 m and vertical errors of ~9 m. Glacier surface elevation for this flight was calculated by subtracting aircraft terrain clearance measured by the radio-echo sounder from the absolute altitude of the aircraft determined by dGPS. Glacier bed elevation was then computed by subtracting the radar-derived ice thicknesses from the surface elevation. Full details of the survey procedure and data analysis are provided in Dowdeswell and others (2004). Oblique photos of Mittie Glacier during the active phase of its surge were also collected during this flight.

A second flight was undertaken by NASA IceBridge on 4 May 2012, which closely followed the path of the April 2000 flight (Fig. 1). Ice thickness was measured with the Multichannel Coherent Data Depth Sounder (MCoRDS) airborne radio-echo sounding system, operating at a frequency of 180–210 MHz. The L2 Ice Thickness V001 dataset was downloaded from the Operation IceBridge Data Portal (https://nsidc.org/icebridge/portal/map) (Paden and others, 2010, updated 2019).

The ice thickness measurements were used to compute ice thickness in excess of flotation (H_b) near the terminus of Mittie Glacier for 2000 and 2012, based on the equation provided by Cuffey and Paterson (2010):

$$H_b = H_M - \frac{\rho_w}{\rho_i} H_w \tag{1}$$

where H_M is total ice thickness, ρ_w is the density of water, ρ_i is the density of ice and H_w is water depth (i.e. the difference between sea level and the glacier bed). H_M was computed by subtracting the absolute bed elevation from the surface elevation of the glacier, whereas the absolute bed elevation was used to determine H_w. A density of 1000 kg m^{-3} was used for ρ_w, taking into consideration input of fresh water at the glacier front, and a density of 900 kg m^{-3} was used for ρ_i, taking into consideration crevasses and firn (Cuffey and Patterson, 2010; Cogley and others, 2011; Dalton and others, 2022).

Information on changes in surface elevation of Mittie Glacier over 5-year periods (2000–2004; 2005–2009; 2010–2014) was derived from the study of Hugonnet and others (2021) at a horizontal resolution of 100 m, downloaded from http://maps.theialand.fr. These elevation changes are primarily generated from

analysis of DEMs derived from Advanced Spaceborne Thermal Emission and Reflection Radiometer (ASTER) stereo imagery, as well as from individual scene pairs created for the ArcticDEM. The full methodology is provided by Hugonnet and others (2021).

4. Results

4.1. Surface characteristics

Over the period 1972–1994 the ablation area of Mittie Glacier showed little change in either optical or SAR imagery, and in June 1994 the glacier had a generally smooth surface, little crevassing and a few supraglacial meltwater ponds (Fig. 2a). The glacier terminus generally retreated between the early 1970s and mid-1990s, by ~1.9 km on its eastern side and ~1.6 km on its western side (Figs 3a, d). This is in line with the retreat of most other tidewater glaciers in the region over this period (Cook and others, 2019).

The first visible signs of surging are apparent in a March 1995 JERS-1 image (Fig. 2b), with an increase in backscatter over the lowermost ~5 km of the glacier since the previous SAR scene from June 1994 (Fig. 2a). This was particularly apparent in narrow regions on either side of the main trunk as crevassing occurred in shear margins. The terminus had retreated by ~1 km since June 1994, and extensive new icebergs and disturbed sea-ice mélange were present in front of the glacier.

By early March 1996 bright backscatter was evident across the lowermost ~10 km of the ablation area as the glacier became more crevassed, with distinct shear margins extending up to 15 km up-glacier from the terminus on the southeast side of the main glacier trunk (Fig. 2c). The terminus advanced by ~1.5 km between March 1995 and March 1996, with the advance being slightly more rapid on the western side than the eastern side (Figs 2b, c, 3b, d). Extensive new icebergs and sea-ice mélange were also present at this time. Between 3 March 1996 and 31 May 1996, the terminus advanced by a further ~1 km and became even more crevassed, particularly on the eastern side (Fig. 2d). The shear margin on both sides of the main glacier trunk also extended to the south (up-glacier) by ~5 km over this 3-month

period, and crevassing became extensive across almost the entire ablation area, to a distance of >20 km up-glacier from the terminus.

The terminus continued to advance to reach a maximum extent in 1999, for a total of 7.3 km further forward on the west side of the glacier than in 1994, and 5.5 km further forward on the east side (Figs 3b, d). An overflight in April 2000 showed extensive crevassing across the main glacier trunk, and evidence of drawdown of the glacier surface from its previous level (Fig. 4).

Retreat of the terminus first became evident in summer 2000. The eastern side of the terminus showed the fastest initial retreat, of 3.1 km between 1999 and 2003, followed by a further gradual retreat of 1.3 km between 2003 and 2017 (Figs 3c, d). In contrast, the western side initially retreated by ~1.5 km between 1999 and 2000, but then stayed in a quasi-stable position until 2007, after which it retreated by a total of 5.3 km up until 2017. Widespread supraglacial ponds first became evident across the ablation area of the glacier in optical imagery in summer 2008, caused by crevasses closing and surface meltwater being unable to drain. These ponds reduced in size and extent in later years, together with most evidence of crevassing, with the majority of the ablation area returning to a smooth surface by ~2012.

A very large crevasse was observed ~28 km up-glacier from the terminus for the first time in a Landsat 5 image from 22 August 1996 (Fig. 5a). This formed in summer 1996, because no sign of the crevasse was present in an ERS-1 image from 31 May 1996. The crevasse had an opening of >100 m, and an across-glacier width of ~2.5 km in August 1996. By April 1997 it had reached ~3 km wide, had a maximum opening of ~150 m and stretched from one shear margin to the other across the entire main glacier trunk (Fig. 5b). The crevasse was curved in a slightly up-glacier direction when it first formed, but became increasingly curved in a downstream direction over the next several years due to faster flow in the glacier centre. Figure 5 shows the progression of the crack as it moved a total of 7.4 km between 1997 and 2017; 7.3 km of this occurred between 1997 and 2006, and only 0.1 km between 2007 and 2017. The rates of movement generally declined over time, with displacement of the crevasse centre by 1320 m a^{-1} between 1997 and 1998, 1390 m a^{-1} between 1998 and 1999, 670 m a^{-1} between 1999 and 2000 and 650 m a^{-1}
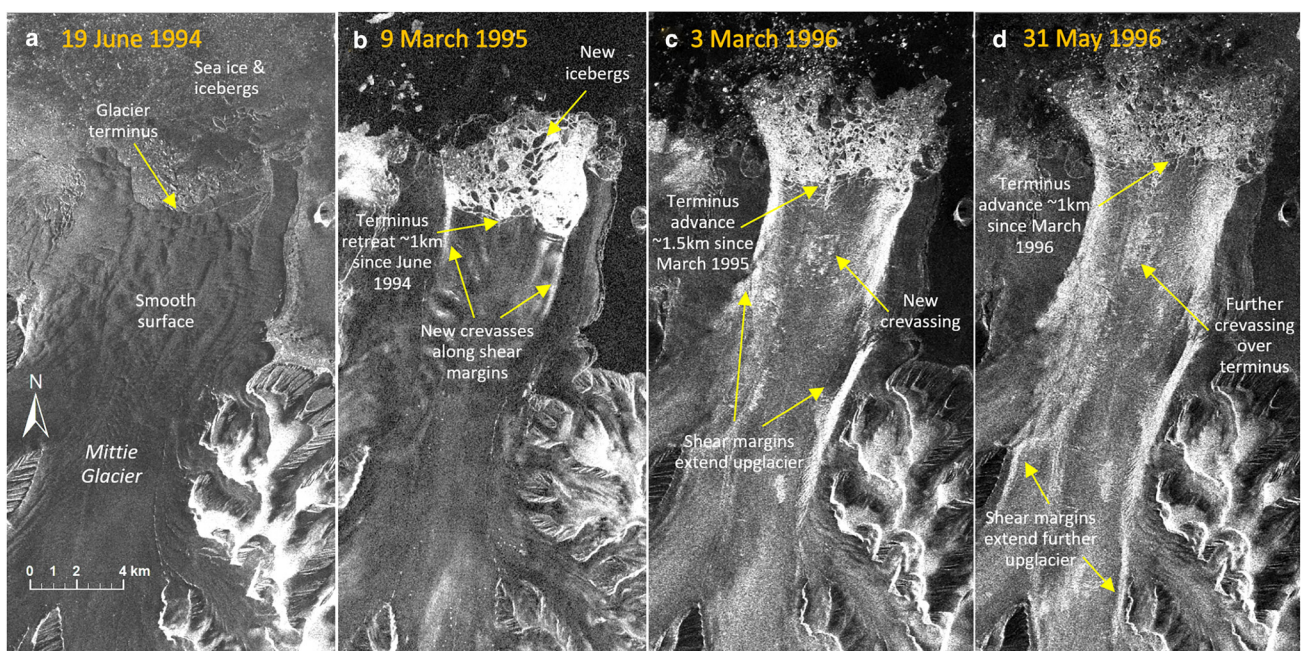

Figure 2. SAR imagery showing the surge phases of Mittie Glacier: (a) prior to main surge initiation; ERS-1, 19 June 1994; (b) near the start of main surge initiation; JERS-1, 9 March 1995; (c) early in the main surge; ERS-1, 3 March 1996; (d) during a period of rapid acceleration and terminus advance; ERS-1, 31 May 1996.
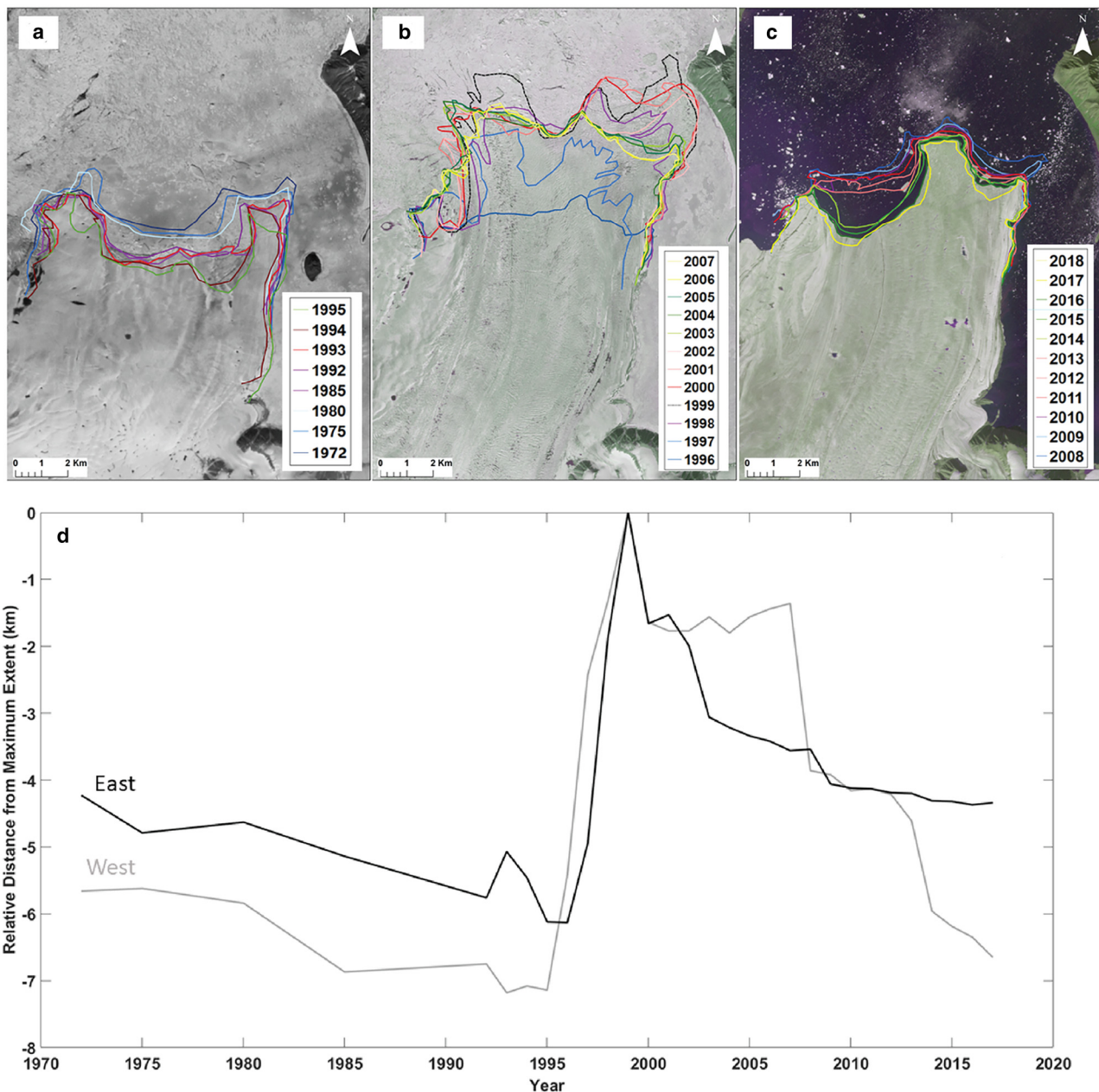
Figure 3. Change in terminus position of Mittie Glacier: (a) before the main surge (1972–1995; background: Landsat 5, 9 July 1993); (b) during the surge (1996–2007; background: ASTER, 3 July 2002); (c) after the surge (2008–2018; background: ASTER, 8 August 2016). (d) Change in terminus extent over the period 1972–2018, relative to the 1999 maximum extent. East (black line) and West (grey line) refer to changes on either side of the terminus shown in Figure 1.

between 2000 and 2001. After 2007 the crevasse gradually closed over the following ~5 years and became a scar on the glacier surface (Fig. 5g).

4.2. Surface velocity

The surface velocity plots show the dramatic changes in dynamics that have occurred at Mittie Glacier since the 1990s (Figs 6, 7). In 1989, the entire glacier was moving slowly, at rates of <100 m a^{-1}, with little spatial variability (Fig. 6). By 1991, the lower part of the terminus was flowing at >100 m a^{-1} (although data coverage was patchy), and by 1992 the lower ~15 km of the glacier was flowing at >200 m a^{-1}. The first evidence of a dramatic change in velocity occurred in March 1996, when the 1-day separated ERS 1/2 images showed values that reached a maximum of ~4800 m a^{-1} (~13 m d^{-1}) within a few kilometres of the terminus. The lower-most 15 km of the glacier was flowing at a rate of >3000 m a^{-1} at this time, with velocities decreasing up-glacier of this.

Lack of images, and lack of coherence between SAR image pairs, precluded the determination of other velocities until 1999–2000, when they exceeded >1000 m a^{-1} across most of the lower 20 km of the glacier (Figs 6, 7). Imagery from 2000 to 2001 still showed similarly high velocities across the lower 20 km of the glacier, with values gradually reducing in an up-glacier direction, to reach <100 m a^{-1} at distances of >40 km up-glacier from the terminus. The velocities up to 2005–2006 showed similar spatial variability, with a peak near the terminus and decrease up-glacier, but with an overall decrease across the main glacier trunk at a rate of ~50–80 m a^{-1} per year.

Velocities in 2006–2007 were dramatically slower than those in 2005–2006 and displayed a different pattern to previous years, with velocities gradually increasing from ~130 m a^{-1} at the terminus to >200 m a^{-1} at 35 km up-glacier from the terminus (Fig. 7). After 2006–2007, the entire lower glacier was essentially stagnant for ~30 km up-glacier from the terminus, although velocities reached >100 m a^{-1} over the 20 km distance up-glacier
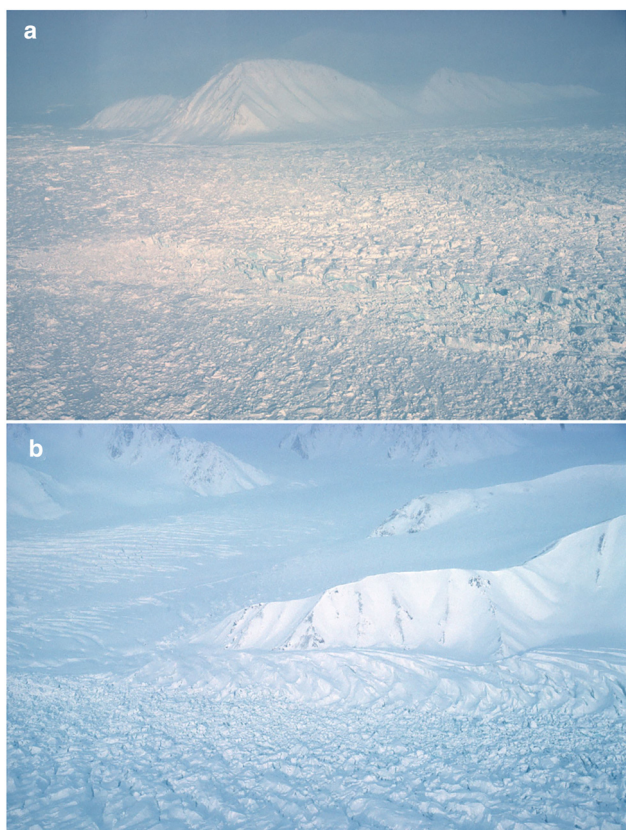
Figure 4. Oblique air photos of Mittie Glacier during its surge, acquired during an overflight in April 2000 (Source: J.A. Dowdeswell). (a) The heavily crevassed main trunk of Mittie Glacier. (b) Extensive crevassing on the main glacier, together with crevassing of a tributary glacier to the east.

from this (i.e. 30–50 km from the terminus). This is evident in the small region of elevated velocities in the far SW part of Mittie Glacier in 2007–2008, with the pattern of stagnation over the lower part of the glacier and higher motion over the upper part of the glacier continuing up to 2018 (Fig. 6).

4.3. Surface and bed topography

The April 2000 SPRI radar data were collected when Mittie Glacier was near its maximum extent and provide surface and bed elevation information for the first ~12 km of the glacier length. Up-glacier of this no bed returns were detectable as the ice became thicker and the surface was heavily crevassed. Over the lower ~3 km of the glacier at this time the bed was close to 200 m below sea level, rising to ~150 m below sea level ~9 km up-glacier from the terminus (Fig. 1b). Surface elevations averaged ~20 m above sea level across the lower ~3 km of the terminus, and gradually increased up-glacier from there, resulting in total ice thicknesses of >200 m at the terminus, and >300 m near the upper part of the April 2000 profile.

Data from the May 2012 IceBridge flight provided complete bed and surface elevation information for a distance of >30 km up-glacier from the terminus (Fig. 1b; note that bed values over the upper 5 km of the transect likely reflect returns from the valley side wall as the flight path deviated from the glacier centreline; Fig. 1a). This profile started ~2.5 km further up-glacier compared to the one in 2000 due to retreat of the terminus, with the lower 1 km of the glacier in 2012 being markedly thinner at ~130–150 m, compared to ~210–220 m at the same location in 2000.

In terms of changes in surface elevation, the airborne profiles show that Mittie Glacier thickened slightly, by a total of ~5–10 m, over its lowermost ~12 km between 2000 and 2012 (Fig. 1b). At a distance of >20 km from the terminus it appears to have
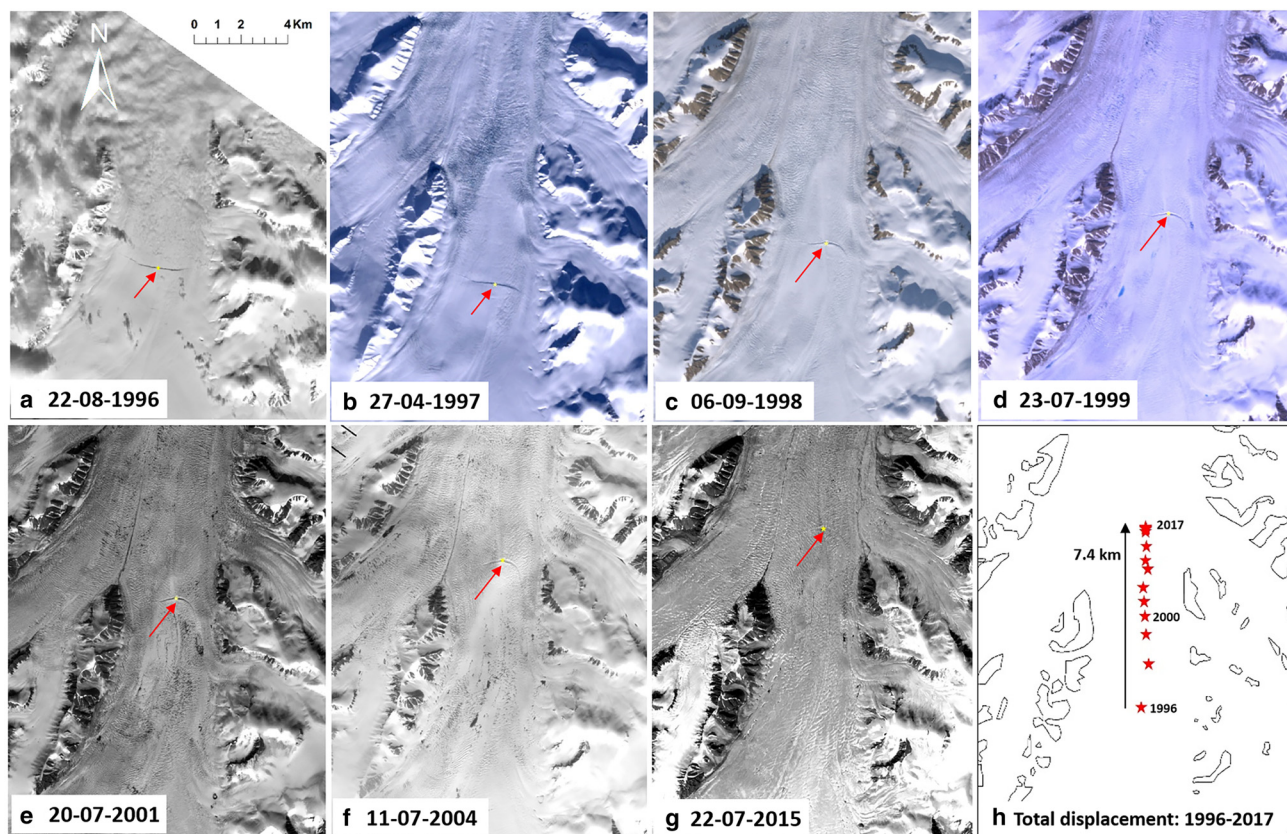

Figure 5. Series of optical satellite images showing progression of a large crevasse on Mittie Glacier (red arrow points to centre) from the start of the main surge in 1996 and its progression up to 2017. Last panel shows total displacement over entire study period of 7.4 km (7.3 km between 1997 and 2006; 0.1 km between 2007 and 2017).
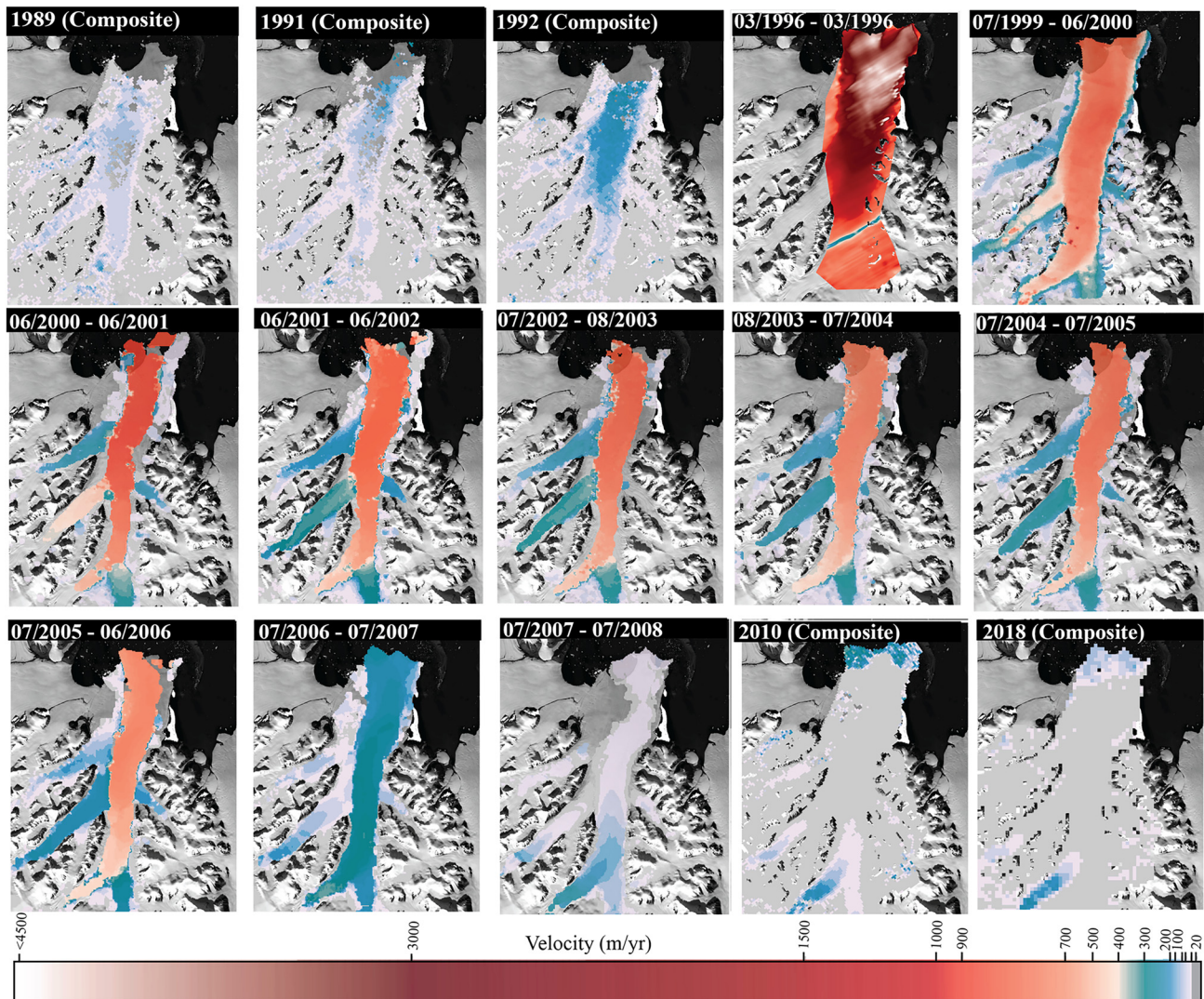
Figure 6. Evolution of velocities through the surge cycle of Mittie Glacier from 1989 to 2018. Composite indicates annual velocities derived from the ITS_LIVE dataset; specific dates refer to image pairs listed in Table 2.

thickened more over this period, by up to ~30 m, although the offset in location of the profiles in this region makes direct comparison between them difficult (Fig. 1a). More details are provided by the 5-year elevation change maps, which show that over the period 2000–2004 the lower ~35 km of the glacier generally thickened, at rates ~0.5 to 1.5 m a^{-1} (Fig. 8). Subsequently, in 2005–2009 there was a marked difference in surface elevation change between the upper and lower parts of the glacier, with the lowermost ~15 km thinning at an average rate of ~1.0 m a^{-1}, compared to thickening at rates of up to 2 m a^{-1} above this. In 2010–2014, these patterns intensified, with thinning over a larger portion of the terminus and more intensive thickening over a larger part of the upper glacier, at rates exceeding 3 m a^{-1} in some locations (Fig. 8).

Parts of the terminus of Mittie Glacier were at or near flotation in April 2000, with the ice thickness in excess of flotation having a median value of ~3.9 m over a distance of 1.9–5.0 km up-glacier from the ice front, and some areas reaching values of <2 m (Fig. 9). Accounting for ice drawdown during the active phase of the surge, the terminus region of Mittie Glacier was likely thinner and, in turn, more buoyant when the surge initiated in the mid-1990s. In 2012, due to thickening of the lower part of the glacier since 2000, values of ice thickness in excess of flotation were higher than in 2000, with a median of ~25.8 m within ~5 km from the 2012 terminus.

5. Discussion

Mittie Glacier has been previously documented as a surge-type glacier (Copland and others, 2003*a*; Sharp and others, 2014; Van Wychen and others, 2016), but from our results we can provide a more detailed analysis of the surge initiation and termination, the changes in surface characteristics caused by the surge, as well as constrain the surge duration. We also contextualize the surge compared to dynamic instabilities observed on other glaciers in the Canadian Arctic and elsewhere.

5.1. Surge initiation

We hypothesize that the surge was subtly initiated at the terminus in the early 1990s, before becoming fully developed in 1995. Although we only have partial velocities for this period, the ITS_LIVE data from 1989 indicate flow speeds of 40–60 m a^{-1} along much of the main trunk of the glacier (Figs 6, 7). These velocities are higher than those observations by previous studies when the glacier is in quiescence (Van Wychen and others, 2016, 2021), and our own data since 2010 (Fig. 6), where flow speeds of <25 m a^{-1} are common. In 1991, velocities over the lowermost 8 km of the terminus had increased to reach values of >100 m a^{-1} in places, and by 1992 they had risen to >200 m a^{-1} across most of the lower glacier (Fig. 6). This difference provides
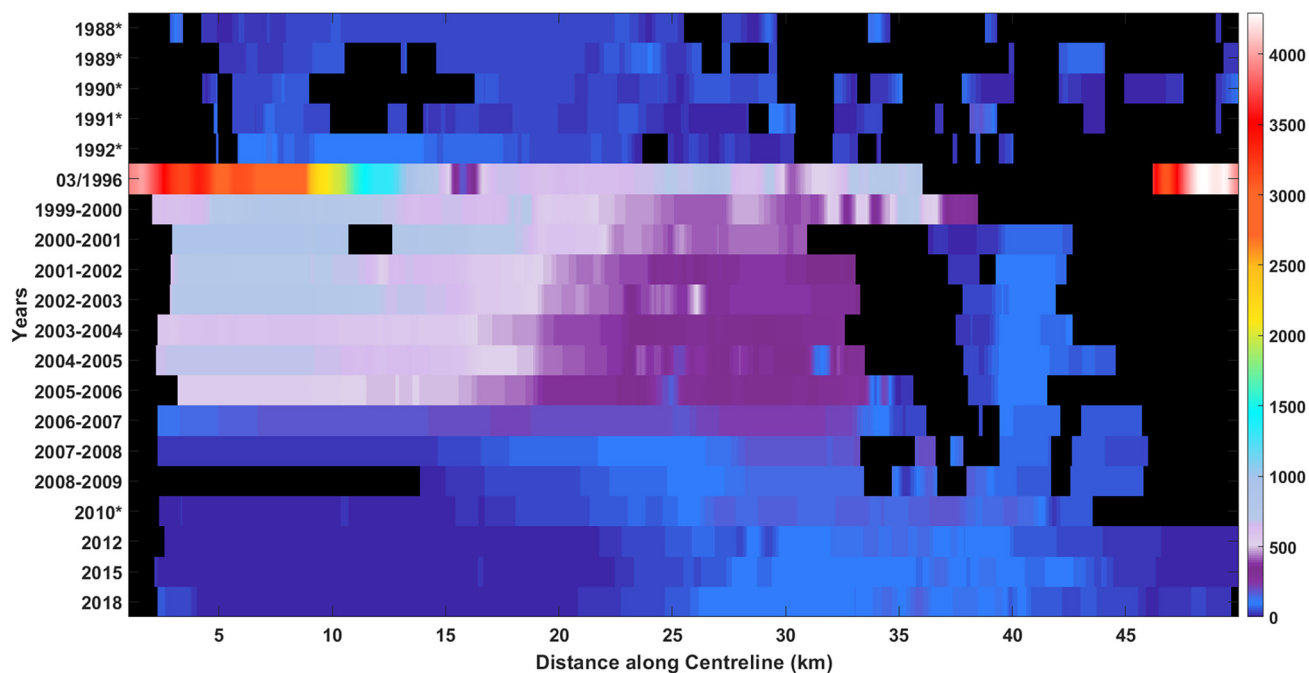
Figure 7. Centreline surface velocity (in m a^{-1}) of Mittie Glacier from 1988 to 2018 along the yellow centreline shown in Figure 1a. Years with an asterisk (*) indicate velocities derived from ITS_LIVE optical image matching; velocities for 03/1996 were derived from SAR offset tracking; annual ranges were derived from optical image feature tracking; single years without an asterisk were derived from SAR speckle tracking.

the first indication of the main surge process starting, although there were no apparent changes in surface characteristics at this time, with SAR backscatter low in June 1994, indicative of little surface crevassing (Fig. 2a).

The first indication of bright backscatter in SAR imagery was in March 1995, indicative of new crevassing and therefore rapid changes in surface velocity, particularly along shear margins either side of the terminus (Fig. 2b). The production of large numbers of new icebergs at the terminus also occurred at this time. No velocity data are available from 1995, but by winter 1996 our data indicate that the surge was fully developed over the entire lower ~20 km of the glacier, with velocities reaching an observed maximum of ~4800 m a^{-1} and the terminus advancing by ~1 km between early March and late May 1996. These peak velocities are the highest ever recorded for a glacier in the Canadian Arctic. Shear margins, caused by the rapid change in velocity between the main glacier trunk and slower margins and tributaries, became extensive during this time and rapidly extended up-glacier in spring 1996. By summer 1996, the formation of the very large crevasse across the glacier width indicates that the surge had extended to a distance of at least 28 km up-glacier from the terminus (Fig. 5).
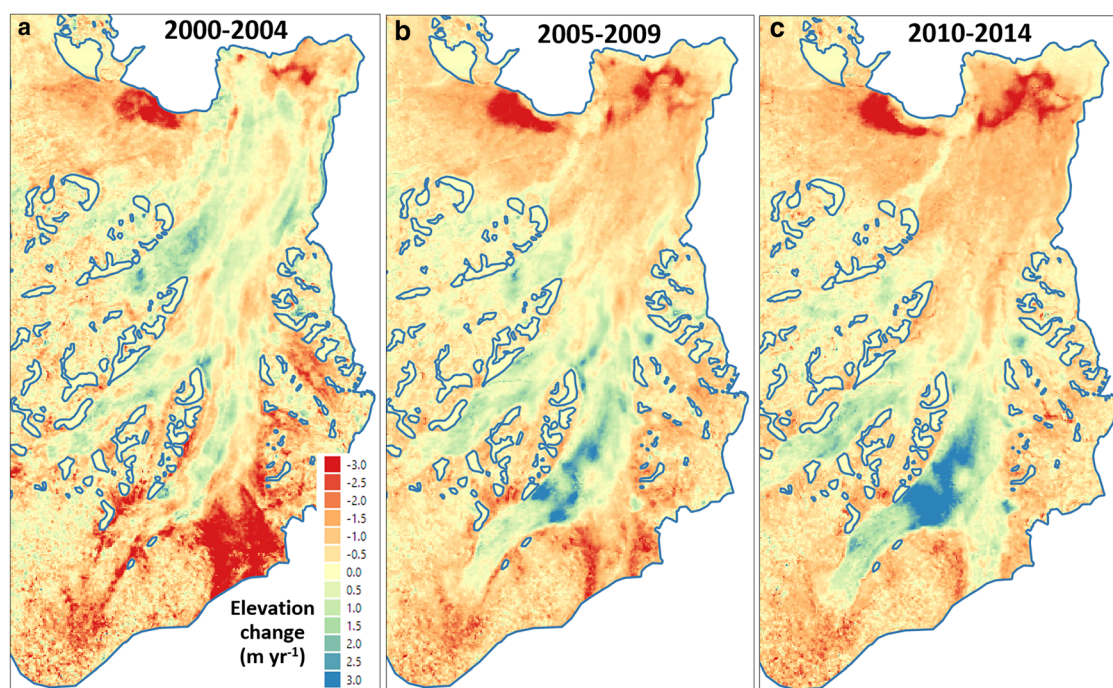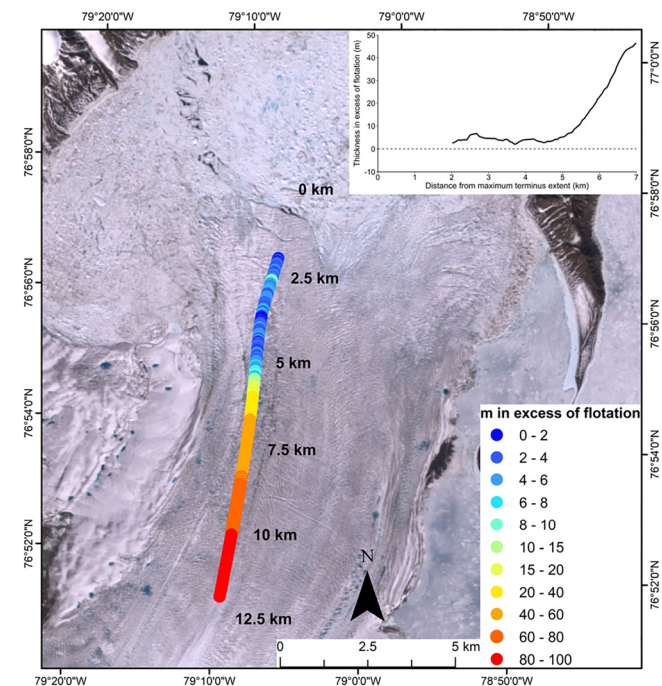

Figure 8.

Figure 9.

In all of the velocity data from 1989 to 1996, significant velocity variability was only observed over the lower ~30 km of Mittie Glacier, with no evidence of velocity changes above this. We therefore argue that the surge was triggered from a destabilization of the glacier terminus, which then propagated up-glacier. This interpretation is supported by the SAR satellite imagery, which shows a change from a smooth to heavily crevassed surface over the lower 4 km of the glacier between June 1994 and March 1995 (Fig. 2). Crevassing then extended up-glacier between March and May 1996, including the formation of new shear margins, suggesting that the surge propagated up-glacier from the terminus over this time.

The first report of surge initiation at a glacier terminus in the Canadian Arctic was recently made for Iceberg Glacier on western Axel Heiberg Island (Lauzon and others, 2023). In the 1970s, a large portion of Iceberg Glacier's terminus was retreating from a pinning point, which appears to have increased its retreat rate and encouraged extension of the glacier front. This, in turn, resulted in an increase in velocities and thinning over the portion of the terminus that was retreating from the pinning point. Flow speeds at the terminus of Iceberg Glacier increased throughout the 1970s from typical values of <50 to >100 m a^{-1} in 1979–1980. In 1981, parts of the terminus rapidly sped up to reach maximum velocities of ~1500 m a^{-1}, suggesting that the surge initiated there and propagated up-glacier (Lauzon and others, 2023). There have also been reports of surges of marine-terminating glaciers elsewhere in the Arctic that start at the terminus and propagate up-glacier, as opposed to the down-glacier-propagating surges of land-terminating glaciers with a well-defined surge front (Sevestre and others, 2018). Examples include Monacobreen in Svalbard (Murray and others, 2003), Aavatsmarkbreen and Wahlenbergbreen in Svalbard (Sevestre and others, 2018), and Harald Moltke Brae in NW Greenland (Müller and others, 2021).

From a process perspective, we argue that the subtle speed-up observed at Mittie Glacier in the early 1990s is an important precursor to the initiation of the main surge in 1995. The radio-echo sounding measurements in 2000 indicate that the lower ~5 km of the terminus was near flotation, with some parts within 2 m of flotation, indicating high buoyancy (Fig. 9). If the surface elevation changes observed since 2010 are indicative of long-term quiescent conditions (Fig. 8c), then the lower ~20 km of the glacier thins during the quiescent phase, meaning that surges initiate once the ice thins enough to become buoyant in the near-terminus region. We suggest that as this happens the glacier began to slowly increase in speed in the early 1990s, inducing further dynamic thinning and ultimately flotation at the terminus, which enabled rapid acceleration and the start of the main surge in 1995. This type of behaviour has been reported elsewhere, such as the surge of Basin-3, Austfonna, Svalbard, which first underwent a multiannual acceleration prior to surge initiation caused by successive mobilization and destabilization of the tidewater terminus, following the failure of a marginal ice plug in 2012 (Dunse and others, 2015). The gradual acceleration preceding the large speedup in 2012 occurred in discrete steps that coincided with consecutive summer melt periods, with surface meltwater reaching a growing portion of the glacier bed and thus providing an efficient heat source through the process of cryo-hydrological warming (i.e. latent heat release during refreezing of meltwater). A portion of the terminus of Basin-3 could have reached buoyancy in 2012 when the surge initiated, followed by an up-glacier propagation of the dynamic instability (McMillan and others, 2014).

Sevestre and others (2018) observed that acceleration of the front of Aavatsmarkbreen and Wahlenbergbreen, also in Svalbard, occurred after a large increase in driving stress in the terminal zone as it retreated from a pinning point, increasing longitudinal extension. Crevasses developed in the terminal zone, allowing surface meltwater and rainwater to access the bed, resulting in flow acceleration and the development of new crevasses upstream from the terminus. The up-glacier propagation of the surge was concurrent with the stepwise expansion of the crevasse field (Sevestre and others, 2018). These patterns are similar to the upward migration of crevasses observed for Mittie Glacier from 1994 to 1996 (Fig. 2).

Significant changes in flow rates, surface morphology and terminus position of a tidewater glacier can occur as part of the 'tidewater glacier cycle', first proposed by Post (1975) based on observations of tidewater glaciers in Alaska. The tidewater glacier cycle is a retreat instability that occurs on grounded tidewater glaciers and is characterized by variations between long periods of very slow terminus advance over centuries to millennia, followed by shorter periods of rapid disintegration and terminus retreat across a submarine overdeepening over decades (Post, 1975; Meier and Post, 1987; Post and others, 2011; Howat and Vieli, 2021). The retreat phase of this cycle is often accompanied by flotation of the terminus region and high rates of calving. What differentiates this process from the dynamic instability of Mittie Glacier is that Mittie does not appear to have been retreating into deeper water as it began to accelerate, and it experienced high rates of terminus advance rather than retreat. In addition, the recent stagnation and terminus retreat of Mittie Glacier could not be explained by the tidewater glacier cycle.

The formation of the very large, glacier-wide, crevasse ~28 km up-glacier from the terminus in summer 1996 (Fig. 5a) is located at the division between fast-moving ice downstream, and slower ice upstream, and reflects the physical manifestation of this sharp velocity gradient. The crevasse formed at the location where basal topography first rises above sea level (Fig. 1b), providing further evidence that basal conditions play a crucial role in the surges of Mittie Glacier. The bed of the lower part of Mittie

Glacier is unusually flat compared to many other glaciers in this region, and lacks basal pinning points that are often found at these other ice masses (Van Wychen and others, 2016, 2021; Dalton and others, 2022). Van Wychen and others (2016, 2021) and Dalton and others (2022) also report that other marine-terminating glaciers along eastern Ellesmere Island experience higher and more variable velocities in their regions which are grounded below sea level, in comparison to up-glacier regions which are grounded above sea level. Studies elsewhere have demonstrated that basal topography can shape where surge initiation takes place, and where speedups and slowdowns occur along a glacier length (Lovell and others, 2018). The results of our work provide further evidence that bed topography plays an important role in modulating and governing surge behaviour within the Canadian Arctic.

5.2. Surge termination

After peak surge velocities were observed in 1996, velocities over the main trunk of Mittie Glacier still exceeded >1000 m a^{-1} until about 2001, after which they gradually slowed until 2006, and then slowed more rapidly in 2007 and 2008 (Figs 6, 7). The centreline velocities shown in Figure 7 provide evidence that the 2001–2006 slowdown occurred over the upper glacier first (>23 km from the terminus), and then progressed down-glacier over time. However, after 2007/08 the pattern of slowdown reversed, with near stagnation over the lower 20 km of the glacier, while velocities remained higher up-glacier of this point, particularly at distances of >25 km from the terminus. These patterns remained essentially constant for the following decade, until the end of our velocity record in 2018 (Fig. 6).

The region between ∼20 and 32 km from the terminus appears to be an important pivot point for the dynamics of the surge. Surge velocities extend little above this, but quiescent velocities are elevated in these upper regions while the surface elevation is increasing (Fig. 8c). In contrast, peak surge velocities of >1000 m a^{-1} only occur below this region, but the ice is essentially stagnant in these lower parts during quiescence and is thinning over time. As discussed in the previous section this corresponds with a steep increase in bed slope, an increase in basal topography from ∼200 m below sea level to ∼150 m above sea level (Fig. 1b), and the location of the large, glacier-wide crevasse (Fig. 5).

As Mittie Glacier surged in the mid-1990s, its terminus advanced by ∼3–4 km between 1996 and 2002. Between 1999 and 2001, the eastern portion of the terminus extended to reach a small island located within the fiord (Fig. 3b). It is at this time that the velocities in the lowermost terminus of Mittie Glacier begin to slow (Fig. 7), and as such this island may play an important role in terms of stabilising the glacier, providing a pinning point and contributing to the surge termination observed thereafter. It is also likely that the drawdown of ice during the surge and the resultant thickening of the lower part of the glacier would have lowered the buoyancy of the terminus region. This region of Mittie Glacier would have eventually stopped floating and become grounded, resulting in an increase in effective pressure and thus lower rates of basal sliding.

5.3. Surge duration

Our velocity record indicates that the surge initiated around 1992, with a subtle speed up in flow rates across the lower glacier, experienced peak velocities in the mid-1990s, and became largely stagnant after 2007. If we take 1992 and 2007 as the surge start and end points, the surge duration would be ∼15 years. Copland and others (2003a) provided evidence for surges lasting at least a decade on other glaciers in the Queen Elizabeth Islands,

but did not have data to precisely constrain surge durations. However, recent studies have provided velocity records that help to quantify surge durations within this region. For example, the records provided by Millan and others (2017) and Van Wychen and others (2021) indicate that Otto Glacier on northern Ellesmere Island experienced surge-like flow speeds of >800 m a^{-1} in 1991, but had transitioned to quiescence by 2013, suggesting a surge length of 22 years. Iceberg Glacier on western Axel Heiberg Island experienced a surge that lasted for 22 years from 1981 to 2003, including a terminus advance of >7 km, velocities up to ∼2300 m a^{-1}, and median trunk-wide surface elevation changes reaching >3 ± 1 m a^{-1} due to the drawdown of ice from the glacier's reservoir area (Lauzon and others, 2023). A detailed study of Split Lake Glacier on Prince of Wales Icefield, further north on Ellesmere Island, indicated that this glacier has likely been undergoing a slow surge with a duration of 50+ years (Van Wychen and others, 2022). Medrzycka and others (2019) showed that Good Friday Glacier on western Axel Heiberg Island advanced continuously for ⍰⍰⍰70 years between 1948 and 2018, totalling to ∼9.3 km. Similarly, a recent study by Lauzon and others (2024) indicated that Airdrop Glacier, located <150 km north of Good Friday, also advanced continuously by ∼6 km from 1950 to 2021.

Whereas the 15-year surge of Mittie Glacier is shorter than these other dynamic instabilities, all of these findings highlight the long timescales over which such instabilities manifest themselves within the Canadian Arctic. Our results show that surges in this region can be rather pronounced and expand upon characterization of the wide spectrum of glacier dynamic behaviour in the Canadian Arctic. Previous studies suggest that surges in Svalbard last for an average of 3–10 years (Dowdeswell and others, 1991), but from the results presented here and the studies mentioned above, it seems that average active phase length may be longer in the Canadian Arctic.

We do not have any information concerning the duration of the quiescent phase of Mittie Glacier, but know that it must be >40 years based on the lack of surge features in an air photo from 1959 and satellite images from prior to the 1990s.

6. Conclusions

Mittie Glacier underwent an approximately 15-year long surge event, which began around 1992 and ended around 2007. The surge initiated at the terminus and propagated up-glacier, with a large glacier-wide crevasse indicating the boundary between fast moving ice downstream that was grounded below sea level, and slow moving ice upstream that was grounded above sea level. The combination of terminus initiation, up-glacier propagation, an extensive region of the glacier grounded below sea level and surface elevations close to sea level strongly suggest that the surge of Mittie Glacier was triggered by flotation of the terminus. It is unknown whether the resulting surge was driven by changes in basal water pressure or changes in basal thermal regime, but the long duration of the active phase is most similar to thermally controlled surges previously reported in Svalbard (Dowdeswell and others, 1991; Fowler and others, 2001; Murray and others, 2003, Dunse and others, 2011). However, dynamic instabilities in the Canadian Arctic can last significantly longer than what has been reported for Svalbard and elsewhere (Medrzycka and others, 2019; Van Wychen and others, 2022; Lauzon and others, 2024), suggesting that the processes regulating surging within these regions may not be identical.

In terms of surge intensity, the peak velocities (4800 m a^{-1}) determined for Mittie Glacier are the fastest flow speeds that have been reported for any glacier in the Canadian Arctic, and provide further evidence of the diverse ways that dynamic instabilities are manifested within the region. Furthermore, the surge of Mittie Glacier was

more extensive than anywhere else previously reported in the Canadian Arctic, with velocity variability occurring over a portion of the glacier that is ~30 km in length and ~5.5 km in width.

Further work would be useful to understand the causes of surge initiation at the terminus of Mittie Glacier, particularly in relation to changes in surface elevation, mass balance and internal and basal thermal conditions. There are insufficient data to reconstruct these patterns for the surge reported here, but ongoing monitoring will hopefully provide information that will help to better understand the evolution of the glacier during the current quiescent phase and when it may next surge.

References

Bingham RG, Nienow PW and Sharp MJ (2003) Intra-annual and intra-seasonal flow dynamics of a High Arctic polythermal valley glacier. *Annals of Glaciology* **37**(1), 181–188. doi: 10.3189/172756403781815762

Ciracì E, Velicogna I and Swenson S (2020) Continuity of the mass loss of the world's glaciers and ice caps from the GRACE and GRACE Follow-On missions. *Geophysical Research Letters* **47**(9), e2019GL086926. doi: 10.1029/2019gl086926

Cogley JG and 10 others (2011) *Glossary of Glacier Mass Balance and Related Terms*. Paris: UNESCO/IHP. doi: 10.5167/UZH-53475

Colgan W and 6 others (2016) Glacier crevasses: observations, models, and mass balance implications. *Reviews of Geophysics* **54**(1), 199–161. doi: 10.1002/2015RG000504

Cook A and 7 others (2019) Atmospheric forcing of rapid marine-terminating glacier retreat in the Canadian Arctic Archipelago. *Science Advances* **5**(3), 11pp, eaau8507. doi: 10.1126/sciadv.aau8507

Copland L, Sharp M and Dowdeswell J (2003*a*) The distribution and flow characteristics of surge-type glaciers in the Canadian High Arctic. *Annals of Glaciology* **36**, 73–81. doi: 10.3189/172756403781816301

Copland L, Sharp M and Nienow P (2003*b*) Links between short-term velocity variations and the subglacial hydrology of a predominantly cold polythermal glacier. *Journal of Glaciology* **49**(166), 337–348. doi: 10.3189/172756403781816301

Cuffey KM and Paterson WSB (2010) *The Physics of Glaciers*, 4th Edn. Oxford: Butterworth-Heinemann.

Dalton A, Van Wychen W, Copland L, Gray L and Burgess D (2022) Seasonal and multiyear flow variability on the Prince of Wales Icefield, Ellesmere Island, 2009–2019. *Journal of Geophysical Research Earth Surface* **127**(4), e2021JF006501. doi: 10.1029/2021JF006501

Dowdeswell JA, Hamilton GS and Hagen JO (1991) The duration of the active phase on surge-type glaciers: contrasts between Svalbard and other regions. *Journal of Glaciology* **37**, 388–400. doi: 10.3189/S0022143000005827

Dowdeswell JA, Hodgkins R, Nuttall A-M, Hagen JO and Hamilton GS (1995) Mass balance change as a control on the frequency and occurrence of glacier surges in Svalbard, Norwegian High Arctic. *Geophysical Research Letters* **22**, 2909–2912. doi: 10.1029/95GL02821

Dowdeswell JA, Benham TJ, Gorman MR, Burgess D and Sharp MJ (2004) Form and flow of the Devon Island Ice Cap, Canadian Arctic. *Journal of Geophysical Research Earth Surface* **109**(F02002), 14pp. doi: 10.1029/2003JF000095

Dunse T and 5 others (2015) Glacier-surge mechanisms promoted by a hydro-thermodynamic feedback to summer melt. *The Cryosphere* **9**, 197–215. doi: 10.5194/tc-9-197-2015

Dunse T, Greve R, Schuler TV and Hagen JO (2011) Permanent fast flow versus cyclic surge behaviour: numerical simulations of the Austfonna ice cap, Svalbard. *Journal of Glaciology* **57**(202), 247–259. doi: 10.3189/002214311796405979

Fowler AC, Murray T and Ng FSL (2001) Thermally controlled glacier surging. *Journal of Glaciology* **47**(159), 527–538. doi: 10.3189/172756501781831792

Gardner AS and 6 others (2018) Increased West Antarctic and unchanged East Antarctic ice discharge over the last 7 years. *The Cryosphere* **12**(2), 521–547. doi: 10.5194/tc-12-521-2018

Gardner AS, Fahnestock MA and Scambos TA (2021) *ITS_LIVE Regional Glacier and Ice Sheet Surface Velocities*. Boulder: Data archived at National Snow and Ice Data Center. doi: 10.5067/6II6VW8LLWJ7

Harcourt WD and 9 others (2020) Subglacial controls on dynamic thinning at Trinity-Wykeham Glacier, Prince of Wales Ice Field, Canadian Arctic. *International Journal of Remote Sensing* **41**, 1191–1213. doi: 10.1080/01431161.2019.1658238

Hattersley-Smith G (1964) Rapid advance of glacier in northern Ellesmere Island. *Nature* **201**(4915), 176. doi: 10.1038/201176a0

Hattersley-Smith G (1969) Recent observations on the surging Otto Glacier, Ellesmere Island. *Canadian Journal of Earth Sciences* **6**(4), Part 2, 883–889. doi: 10.1139/e69-090

Heid T and Kääb A (2012) Repeat optical satellite images reveal widespread and long term decrease in land-terminating glacier speeds. *The Cryosphere* **6**(2), 467–478. doi: 10.5194/tc-6-467-2012

Howat I and Vieli A (2021) Tidewater glaciers. In Fowler A and Ng F (eds). *Glaciers and Ice Sheets in the Climate System*. Zurich: Springer Nature Switzerland AG, pp. 79–91. doi: 10.1007/978-3-030-42584-5_4

Hugonnet R and 10 others (2021) Accelerated global glacier mass loss in the early twenty-first century. *Nature* **592**, 726–731. doi: 10.1038/s41586-021-03436-z

Iken A (1974) Velocity fluctuations of an arctic valley glacier, a study of the White Glacier, Axel Heiberg Island, Canadian Arctic Archipelago. *Axel Heiberg Island Research Reports, Glaciology* **5**, 123 pp.

Kääb A, Bazilova V, Leclercq PW, Mannerfelt ES and Strozzi T (2023) Global clustering of recent glacier surges from radar backscatter data, 2017–2022. *Journal of Glaciology* **69**(277), 1515–1523. doi: 10.1017/jog.2023.35

Lauzon B and 5 others (2023) Dynamics throughout a complete surge of Iceberg Glacier on western Axel Heiberg Island, Canadian High Arctic. *Journal of Glaciology* **69**(277), 1333–1350. doi: 10.1017/jog.2023.20

Lauzon B, Copland L, Van Wychen W, Kochtitzky W and McNabb R (2024) Evolution of the dynamics of Airdrop Glacier, western Axel Heiberg Island, over a seven-decade-long advance. *Arctic Science* **10**(1), 48–68. doi: 10.1139/AS-2022-0045

Lenaerts JTM and 5 others (2013) Irreversible mass loss of Canadian Arctic Archipelago glaciers. *Geophysical Research Letters* **40**, 870–874. doi: 10.1002/grl.50214

Lovell AM, Carr JR and Stokes CR (2018) Topographic controls on the surging behaviour of Sabche Glacier, Nepal (1967 to 2017). *Remote Sensing of Environment* **210**, 434–443. doi: 10.1016/j.rse.2018.03.036

McMillan M and 14 others (2014) Rapid dynamic activation of a marine-based Arctic ice cap. *Geophysical Research Letters* **41**(24), 8902–8909. doi: 10.1002/2014GL062255

Medrzycka D, Copland L, Van Wychen W and Burgess D (2019) Seven decades of uninterrupted advance of Good Friday Glacier, Axel Heiberg Island, Arctic Canada. *Journal of Glaciology* **65**(251), 440–452. doi: 10.1017/jog.2019.21

Meier MF and Post A (1969) What are glacier surges? *Canadian Journal of Earth Sciences* **6**(4), 807–817. doi: 10.1139/e69-081

Meier MF and Post A (1987) Fast tidewater glaciers. *Journal of Geophysical Research: Solid Earth* **92**(B9), 9051–9058. doi: 10.1029/JB092iB09p09051

Millan R, Mouginot J and Rignot E (2017) Mass budget of the glaciers and ice caps of the Queen Elizabeth Islands, Canada, from 1991 to 2015. *Environmental Research Letters* **12**(2), 024016. doi: 10.1088/1748-9326/aa5b04

Müller F (1969) Was the Good Friday Bay glacier on Axel Heiberg Island surging? *Canadian Journal of Earth Sciences* **6**(4), Part 2, 891–894. doi: 10.1139/e69-091

Müller L and 8 others (2021) Surges of Harald Moltke Bræ, north-west Greenland: seasonal modulation and initiation at the terminus. *The Cryosphere* **15**, 3355–3375. doi: 10.5194/tc-15-3355-2021

Murray T, Strozzi T, Luckman A, Jiskoot H and Christakos P (2003) Is there a single surge mechanism? Contrasts in dynamics between glacier surges in Svalbard and other regions. *Journal of Geophysical Research Solid Earth* **108**(B5), 2237. doi: 10.1029/2002JB001906

Noël B and 5 others (2018) Six decades of glacial mass loss in the Canadian Arctic Archipelago. *Journal of Geophysical Research Earth Surface* **123**, 1430–1449. doi: 10.1029/2017JF004304

Ommanney CSL (1969) A study in glacier inventory: the ice masses of Axel Heiberg Island, Canadian Arctic Archipelago. *Axel Heiberg Island Research Reports, Glaciology* 3, 105pp.

Paden J, Li J, Leuschen C, Rodriguez-Morales F and Hale R (2010, updated 2019) *IceBridge MCoRDS L2 Ice Thickness, Version 1 [Data Set]*. Boulder, CO, USA: NASA National Snow and Ice Data Center Distributed Active Archive Center. doi: 10.5067/GDQ0CUCVTE2Q

Post A (1975) *Preliminary Hydrography and Historic Terminal Changes of Columbia Glacier, Alaska, United States Geological Survey, Hydrologic Atlas, HA559*. Reston: U.S. Geological Survey. doi: 10.3133/ha559

Post A, O'Neel S, Motyka RJ and Streveler G (2011) A complex relationship between calving glaciers and climate. *Eos, Transactions American Geophysical Union* 92(37), 305–306. doi: 10.1029/2011EO370001

Schaffer N, Copland L and Zdanowicz C (2017) Ice velocity changes on Penny Ice Cap, Baffin Island, since the 1950s. *Journal of Glaciology* 63(240), 716–730. doi: 10.1017/jog.2017.40

Sevestre H and 6 others (2018) Tidewater glacier surges initiated at the terminus. *Journal of Geophysical Research: Earth Surface* 123(5), 1035–1051. doi: 10.1029/2017JF004358

Sevestre H and Benn DI (2015) Climatic and geometric controls on the global distribution of surge-type glaciers: implications for a unifying model of surging. *Journal of Glaciology* 61(228), 646–662. doi: 10.3189/2015JoG14J136

Sharp M and 12 others (2014) Remote sensing of recent glacier changes in the Canadian Arctic. In Kargel JS, Leonard GJ, Bishop MP, Kääb A and Raup BH (eds), *Global Land Ice Measurements from Space*, Ch. 9. Berlin: Springer, pp. 205–228. doi: 10.1007/978-3-540-79818-7_9

Short NH and Gray AL (2005) Glacier dynamics in the Canadian High Arctic from RADARSAT-1 speckle tracking. *Canadian Journal of Remote Sensing* 31(3), 225–239. doi: 10.5589/m05-010

Strozzi T, Luckman A, Murray T, Wegmuller U and Werner C (2002) Glacier motion estimation using SAR offset-tracking procedures. *IEEE Transactions on Geoscience and Remote Sensing* 40, 2384–2391. doi: 10.1109/TGRS.2002.805079

Thomson L and Copland L (2018) Changing contribution of peak velocity events to annual velocities following a multi-decadal slowdown at White Glacier. *Annals of Glaciology*, 58(75pt2), 145–154. doi: 10.1017/aog.2017.45

Van Wychen W and 6 others (2014) Glacier velocities and dynamic ice discharge from the Queen Elizabeth Islands, Nunavut, and Canada. *Geophysical Research Letters* 41(2), 484–490. doi: 10.1002/2013GL058558

Van Wychen W and 6 others (2016) Characterizing interannual variability of glacier dynamics and dynamic discharge (1999–2015) for the ice masses of Ellesmere and Axel Heiberg Islands, Nunavut, Canada. *Journal of Geophysical Research Earth Surface* 121(1), 39–63. doi: 10.1002/2015JF003708

Van Wychen W and 5 others (2021) RADARSAT-2 derived glacier velocities and dynamic discharge estimates for the Canadian High Arctic: 2015–2020. *Canadian Journal of Remote Sensing* 46(6), 695–714. doi: 10.1080/07038992.2020.1859359

Van Wychen W, Halle DAM, Copland L and Gray L (2022) Anomalous surface elevation, velocity and area changes of Split Lake Glacier, western Prince of Wales Icefield, Canadian High Arctic. *Arctic Science* 8(4), 1288–1304. doi: 10.1139/AS-2021-0039

Werner C, Wegmuller U, Strozzi T and Wiesmann A (2005) Precision estimation of local offsets between pairs of SAR SLCs and detected SAR images. *Proceedings, IEEE International Geoscience and Remote Sensing Symposium, IGARSS '05*, pp. 4803–4805. doi: 10.1109/IGARSS.2005.1526747